

Highly catalytic cross-stacked superaligned carbon nanotube sheets for iodine-free dye-sensitized solar cells

Feng Hao,^a Zheng Wang,^b Qiang Luo,^a Jun Lou,^c Jianbao Li,^{ad} Jiaping Wang,^{*b} Shoushan Fan,^b Kaili Jiang^b and Hong Lin^{*a}

Received 31st July 2012, Accepted 4th September 2012

DOI: 10.1039/c2jm35095e

Searching for suitable platinum-free electrocatalysts toward novel iodine-free redox couples is of vital importance for further cost reduction and large-scale implementation of dye-sensitized solar cells (DSCs). Herein, cross-stacked superaligned carbon nanotube (CSCNT) sheets were incorporated as efficient economical cathodes in organic disulfide/thiolate redox electrolyte mediated DSCs. Electrochemical characterization revealed that the CSCNT sheets exhibited notably higher electrocatalytic activity toward the disulfide/thiolate redox shuttle over that of ubiquitous platinized cathodes, featuring a significantly decreased charge transfer resistance (*ca.* 1.26 Ω cm²) and a 4-fold attenuated apparent activation energy (*ca.* 6.90 kJ mol⁻¹) for disulfide reduction, as well as excellent electrochemical stability. Such a superior electrocatalytic activity was mainly attributed to the synergistic effect of the high specific surface area, relatively open structure for electrolyte accessibility and defect-rich CSCNT cathode. A device incorporating a CSCNT cathode confers a high fill factor of 0.67 and power conversion efficiencies up to 5.81%, which are significantly higher than 0.54 and 4.54% for that with a sputtered Pt cathode. Our investigations demonstrate not only the attractive feasibility of replacing scarce platinum cathodes with abundant carbon materials for novel iodine-free electrolytes, but also the importance of suitable catalyst redox coupling for progress in developing low-cost and high-efficiency DSCs.

1. Introduction

Boosted by the urgent need for inexpensive renewable energies and the increasingly global environmental concern,¹ dye-sensitized solar cells (DSCs) have emerged as a credible alternative to solid-state p-n junction photovoltaic devices by virtue of their great potential to afford solar electricity from resource-abundant raw materials and energy-saving device processing.²⁻⁴ Currently, certified record power conversion efficiencies up to 11% have been achieved in conjunction with a polypyridylruthenium complex sensitizer and an organic electrolyte containing a I⁻/I₃⁻ redox couple.⁵ Nevertheless, there are substantial drawbacks to this benchmark I⁻/I₃⁻ redox shuttle, hindering its practical application,⁶ which mainly include (i) corrosiveness towards

most metal substrates or metallic current collectors, (ii) a large mismatch between its oxidation potential (0.35 V *versus* the normal hydrogen electrode (NHE)) and its dye oxidation potential (\sim 1.0 V *versus* NHE), limiting the achievable open-circuit voltage (V_{oc}) and (iii) competitive absorption of visible light by triiodide species, which will be more significant in back-illuminated devices based on metal substrates, or devices with ionic liquid electrolytes containing a much higher iodide/iodine concentration.⁷ Clearly, the development of non-corrosive redox mediators,⁸⁻¹⁷ with reduced mismatch between the oxidation potential of the dye and the redox couple, is of vital importance, not only to enhance the power conversion efficiency (PCE), but also to promote the successful commercialization of such photovoltaic technology.

In this context, Wang *et al.* reported a promising organic disulfide/thiolate redox couple, 5,5'-dithiobis(1-methyltetrazole)/1-methyltetrazole-5-thiolate (T₂/T⁻). A PCE up to 6.4% was achieved in conjunction with a Z907Na sensitizer under standard illumination conditions (AM 1.5G, 100 mW cm⁻²).¹⁷ Subsequently, this organic thiolate/disulfide redox couple has attracted special interest due to its negligible corrosion properties in combination with weak visible light absorption and acceptable conversion efficiency.¹⁸⁻²² However, conventional planar platinum cathodes showed poor catalytic activity toward this

^aState Key Laboratory of New Ceramics & Fine Processing, Department of Materials Science and Engineering, Tsinghua University, Beijing 100084, P. R. China. E-mail: hong-lin@tsinghua.edu.cn

^bState Key Laboratory of Low-Dimensional Quantum Physics, Department of Physics and Tsinghua-Foxconn Nanotechnology Research Center, Tsinghua University, Beijing 100084, P. R. China. E-mail: jpwang@mail.tsinghua.edu.cn

^cMechanical Engineering and Materials Science, Rice University, 6100 Main St, Houston, Texas 77005, USA

^dCollege of Materials Science and Chemical Engineering, Hainan University, Haikou 570228, P. R. China

iodine-free redox couple, thus resulting in a poor fill factor (FF) and a relatively moderate PCE. Such a low FF associated with sulfur-functionalized redox mediators most likely results from the adsorption of sulfur atoms on the cathode surface and thus, slow catalytic reduction of the oxidized species at the platinum cathode.^{17,20,21} Therefore, it is imperative to seek suitable Pt-free catalysts for this promising redox shuttle, especially taking into consideration the low abundance (0.0037 ppm) and high cost (US\$50 per gram) of platinum resources.^{23–33} To this end, inorganic cobalt sulfide (CoS) was firstly introduced and showed better catalytic and photovoltaic performance than ubiquitous platinized cathodes in conjunction with this disulfide/thiolate electrolyte.¹⁸ Sun *et al.* recently reported that organic poly(3,4-ethylenedioxythiophene) (PEDOT) exhibited significant improvement in its electrocatalytic activity towards this sulfide-mediator, leading to a higher PCE of 6.0% in combination with an organic dye (TH305).¹⁹ Further PCE enhancement up to 7.9% was obtained recently by judicious modification of the electrolyte composition and the PEDOT cathode–electrolyte interface.²² More recently, inorganic tungsten carbide (WC), molybdenum sulfide (MoS₂) and tungsten sulfide (WS₂) were reported as viable cathode catalysts for triiodide-to-iodide, as well as disulfide-to-thiolate reduction in DSCs and a significant improvement in the FF in the latter case was observed.^{20,34} Carbonaceous materials have also been investigated due to their low costs and high conductivities. Wu *et al.* reported graphite sheets as the substrate and catalytic material for the disulfide/thiolate redox couple, demonstrating a PCE of 4.79% compared with 3.97% for a platinum cathode under similar experimental conditions.²¹

Carbon nanotubes (CNTs), a unique emerging nanoscale material with the combined advantages of large surface area, high electrical conductivity and chemical stability, have recently attracted much attention as a practical alternative Pt-free cathode in DSCs and exhibited reasonable performance.^{27,30,35–41} Specifically, aligned multi-walled carbon nanotube (MWCNT) arrays have been widely used to replace platinum cathodes to catalyze the reduction of triiodide in DSCs, with the target of better performance and lower material cost.^{35,40–44} However, studies on the exploration of these aligned CNT electrodes in iodine-free electrolytes were quite sparse. Recently, vertically aligned single-walled carbon nanotubes (VASWCNTs) have been successfully implemented as efficient platinum-free cathodes in sulfide-mediated DSCs. Electrochemical impedance spectroscopy (EIS) results indicated that the VASWCNT cathode exhibited a notably higher electrocatalytic activity than that of the conventional Pt cathode, accompanied by a greatly attenuated charge-transfer resistance (R_{ct}) across the cathode–electrolyte interface.⁴⁵

Furthermore, it is worth mentioning that superaligned carbon nanotube (SACNT) arrays, first grown on silicon wafers using the chemical vapor deposition (CVD) method,⁴⁶ can be easily converted into continuous films by a convenient cross-stacking technique, with the aligned CNTs parallel to the direction of drawing.⁴⁷ Such SACNT films opened up new possibilities for fabricating CNT devices with uniform properties on a large scale, which are currently attracting worldwide interest in the field of nanoscience and nanotechnology. Novel applications of these freestanding thin films have been developed, such as transparent conductive films, electron sources, transmission electron

microscopy (TEM) grids, loudspeakers, touch panels, electrodes for lithium-ion batteries and supercapacitors, and so on.⁴⁸ These exciting applications of SACNTs inspired us to explore their electrochemical utilization as an inexpensive cathode in DSCs with the recently developed disulfide/thiolate redox shuttle, by exploiting their superior conductivity and chemical stability. Herein, we show that multilayers of free-standing aligned CNT films were cross-stacked together to form a robust CSCNT sheet, and pieces of laser-cut CSCNT sheet were transferred and attached onto transparent conducting glasses as efficient low-cost, platinum-free cathodes in iodine-free DSCs, featuring a notably higher electrocatalytic activity toward the disulfide/thiolate redox shuttle over that of the conventional planar Pt cathode.

2. Experimental

Superaligned CNT arrays comprising CNTs with a length around 280 μm were synthesized in batches on 4 inch silicon wafers with iron as the catalyst in a 4 inch low-pressure chemical vapor deposition (LPCVD) system using iron thin film and acetylene as the catalyst and the precursor for CNT growth, respectively.⁴⁹ The superaligned CNT films were directly drawn out from the arrays and stacked onto stainless steel holders layer by layer. The cross-stacked sheets were shrunk and tightened by dipping them into solvents, such as ethanol or acetone. After the solvent was evaporated, the sheets were laser-cut into small circles with a diameter of 6 mm. With the aid of a small droplet of ethanol, the CNT sheets were finally transferred onto pre-cleaned transparent conducting glass to form robust CSCNT cathodes.

A sputtered platinum cathode was prepared using an ion sputtering coater (SBC-12, KYKY Technology Development Ltd., China) for comparison. The thickness of the obtained Pt film was approximately 50 nm. DSC devices were fabricated according to our previous reports.⁵⁰ TiO₂ electrodes with a configuration of 8 μm transparent layer (20 nm particle diameter) and a 5 μm thick scattering layer (250 nm particle diameter) on an FTO substrate (sheet resistance: 12 Ω per square, Nippon Sheet Glass, Co., Ltd.) were used in this study. The obtained TiO₂ electrodes were dipped into dry ethanol solution containing 5×10^{-4} M [(C₄H₉)₄N]₂[Ru(II)L₂(NCS)₂] (known as N719, where L = 2,2'-bipyridyl-4,4'-dicarboxylic acid, ruthenium TBA535, Solaronix, Switzerland) for 2 h at 50 °C. The dye-sensitized TiO₂ electrodes, CSCNTs and Pt cathodes were assembled to form DSCs by sandwiching a redox couple (T⁻/T₂) electrolyte solution composed of 0.4 M T⁻, 0.4 M T₂, 0.5 M 4-*tert*-butylpyridine, and 0.05 M LiClO₄ in acetonitrile–ethylene carbonate = 6 : 4 (volume ratio). The organic redox couple (T⁻/T₂) was synthesized by the literature method.¹⁷

The morphologies of the obtained CSCNTs were characterized by field emission scanning electron microscopy (FEI-Sirion 200 FESEM, FEI, USA) and transmission electron microscopy (Tecnai F20 TEM, FEI, USA). Raman characterization (633 nm excitation) was performed using a Confocal Raman Microscope (HR800, Horiba Jobin Yvon, France). To assess the corresponding catalytic performance of different counter electrodes, R_{ct} across the cathode–electrolyte interface was investigated by means of EIS with the symmetrical thin-layer cells method. The frequency range was set from 1 Hz to 1 MHz, and the amplitude

of the alternating current was set to 10 mV. The temperatures of those measurements were controlled by a temperature humidity chamber (RP-80A, Beijing Hongzhan Instrument Co., Ltd.) with a temperature resolution of 0.3 °C. The photocurrent–voltage (J – V) characteristics of the DSCs were measured with a digital source meter (2400, Keithley Instruments, USA) under AM 1.5G illumination (100 mW cm⁻²), which was realized by a solar simulator (91192, Oriel, USA, calibrated with a standard crystalline silicon solar cell).

3. Results and discussion

The fabrication procedure for the CSCNT film is schematically illustrated in Fig. 1. As described in the experimental section, a cross-stacked sheet is obtained by sequential stacking along one direction, followed by stacking in its perpendicular direction. In this study, only sheets with a configuration of 50 × 50 layers were used. The thickness of the CSCNT sheet is estimated to be around 3 μm. The molecular structure of the organic disulfide/thiolate redox couple (T₂/T⁻) was also shown in the inset of Fig. 1.

Fig. 2(a) shows a representative SEM image of the as-fabricated CSCNT sheet. These CNTs are generally parallel to each other within the same layer of the sheet, and perpendicular to each other between neighboring layers, due to the controlled drawing direction. This directional arrangement is chosen to maximize the in-plane conductivity, as previously described by a two-dimensional model.⁵¹ It is observed that the individual CNTs had fairly uniform diameters, while most of them formed bundles when drawn out from the super-aligned arrays. The formation of bundles undoubtedly favors the electronic conductivity of the cross-stacked sheets.⁴⁷ The nanoscale spacing between the CNTs contributes a large part of the total volume of the sheet. Such a geometrical structure of the CSCNT possesses the merit of direct electron transport through individual super-aligned nanotubes, as well as rapid redox diffusion in a relatively open structure around the nanotubes. Fig. 2(b) and (c) show typical TEM images of the CSCNT sheet after sonication in ethanol and drop casting onto a TEM grid. It is evident from these images that the CNTs typically consist of 6–8 walls with a diameter of *ca.* 8 nm, thus giving rise to a significantly high specific surface area. Due to its repeatability and simplicity in processing, this fabrication technique is highly scalable for industrial manufacturing settings.⁴⁸

Raman spectroscopy, a relatively easy, non-destructive, non-contacting, and quick measurement method to probe the inelastic scattering of light from a sample surface at room

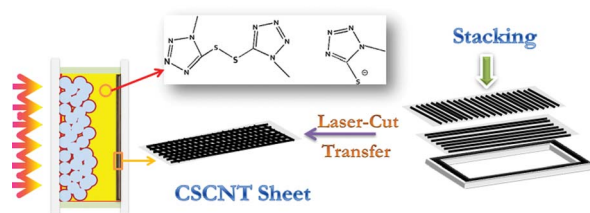


Fig. 1 Schematic illustrations of cross-stacked superaligned CNT films and the DSC device incorporating the CSCNT sheet as cathode material; inset shows the molecular structure of the T₂/T⁻ redox couple.

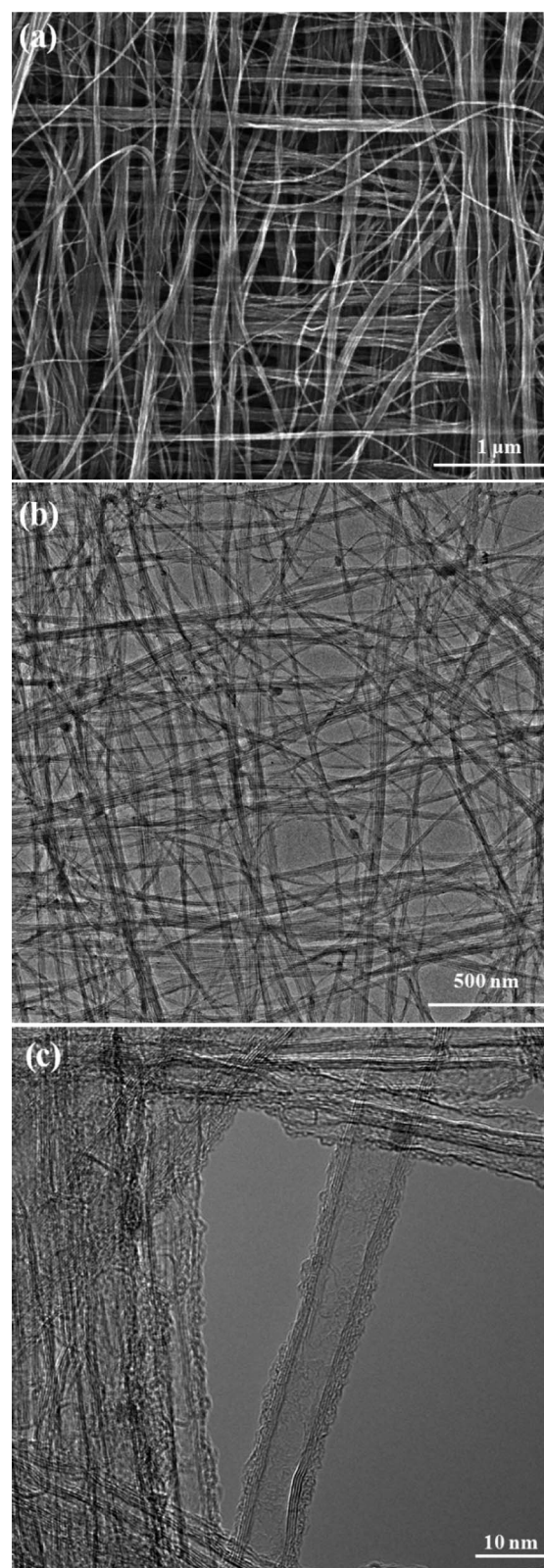


Fig. 2 Representative SEM (a), TEM (b) and HRTEM (c) images of the as-fabricated CSCNT sheet.

temperature and under ambient pressure, was then applied to characterize the quality of the CSCNT sheets. From the Raman characterization (633 nm excitation) of Fig. 3, a D band centred

at a wavenumber of $\sim 1350\text{ cm}^{-1}$ and a D' band at about 1620 cm^{-1} , which are related to disordered and/or turbostratic carbonaceous components, together with a G band, which appeared at a wavenumber of $\sim 1582\text{ cm}^{-1}$ and corresponded to the ordered graphitic structures are observed.⁵² The D and D' bands are defect induced Raman features, which indicates that the CNTs are not highly crystalline graphite. The intensity ratio I_D/I_G for the D band and G band is widely used for characterizing the defect quantity in graphitic materials. It is obvious that these multi-walled CNT sheets show a D/G ratio around 1, suggesting a large amount of defects, such as amorphous carbon residues in the nanotubes and defect-rich edge-planes.⁵³ It is worth noting that such structural defects in CNTs are recognized as important electrocatalytic active sites for the redox reaction, thus facilitating electron-transfer kinetics at the cathode–electrolyte interface, according to recent studies.⁵⁴

The electrocatalytic activity of the as-fabricated CSCNT cathode toward the disulfide/thiolate redox shuttle was systematically investigated by EIS measurement.^{55,56} Fig. 4 presents the representative Nyquist and Bode spectra of symmetrical dummy cells with a CSCNT cathode and the conventional sputtered Pt electrode as a reference. It is generally recognized that in the order of increasing frequency, the impedance response can be attributed to the Warburg diffusion processes in the electrolyte and charge transfer at the cathode–electrolyte interface.⁵⁶ The charge transfer resistance (R_{ct}) can be calculated as half the value obtained from the EIS fitting (the cells employed here were symmetric) multiplied by the geometric surface area of the dummy cell. By fitting with the commonly applied equivalent circuit,⁴⁵ the R_{ct} of the CSCNT cathode, as shown in Table 1, is only $1.26\text{ }\Omega\text{ cm}^2$, which is one order of magnitude lower than that of the conventional Pt cathode ($12.55\text{ }\Omega\text{ cm}^2$) under similar measurement conditions, highlighting the superior electrocatalytic activity of the CSCNT sheet towards disulfide-to-thiolate reduction. Importantly, this value is considerably lower than that of the recently recognized porous PEDOT cathode ($7.8\text{ }\Omega\text{ cm}^2$).²² Compared with our previous study on the VASWCNT cathode ($1.80\text{ }\Omega\text{ cm}^2$),⁴⁵ the CSCNT cathode also exhibits a higher catalytic activity, mainly due to the higher degree of defects in the multi-walled CNT cathode, as demonstrated by the

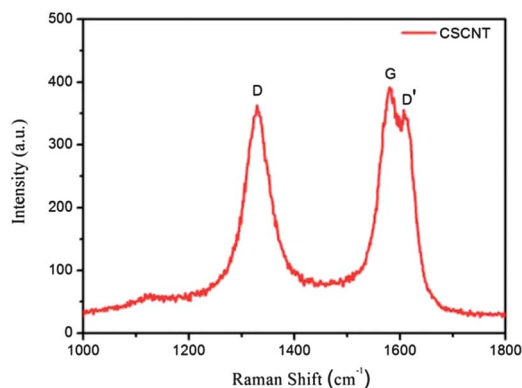


Fig. 3 Raman spectrum of the as-fabricated CSCNT sheets (633 nm excitation), in which the G band appears at 1582 cm^{-1} (graphite), the D band at about 1350 cm^{-1} and the D' band at about 1620 cm^{-1} (defect induced Raman features).

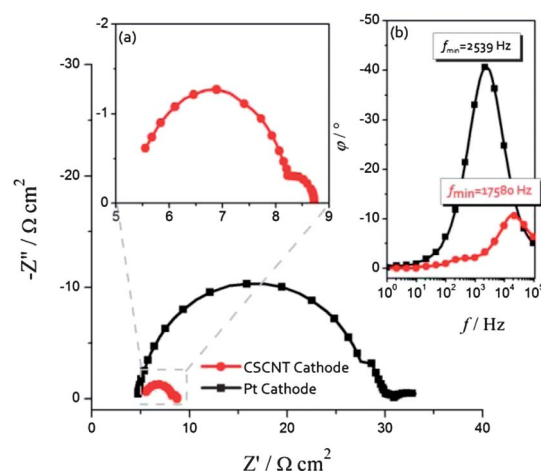


Fig. 4 Representative Nyquist spectra of symmetrical dummy cells with CSCNT cathode and conventional sputtered Pt electrode; inset (a) shows the enlarged view of the Nyquist spectrum for the CSCNT cathode; (b) depicts the corresponding Bode plots for the two different cathodes with an indication of the frequency for the characteristic response peaks. The electrolyte used for the measurements is 0.4 M T_2 , 0.4 M T^- , $0.5\text{ M 4-tert-butylpyridine}$, and 0.05 M LiClO_4 in acetonitrile–ethylene carbonate = $6 : 4$, (volume ratio). The active area of the cells was 0.283 cm^2 .

Raman spectrum.^{54,57} Furthermore, another important parameter in the EIS characterization is the frequency of the characteristic response peaks in the high-frequency regime of the Bode plot (f_{\min}), signifying the electron transfer rate at the cathode–electrolyte interface. As indicated in inset (b) of Fig. 4, the characteristic response peak shifted from 2539 Hz to $17\,580\text{ Hz}$ when changing from the Pt cathode to the CSCNT cathode, demonstrating a considerably faster electron transfer rate across the CSCNT cathode–electrolyte interface with respect to the Pt cathode. In addition, it is also observed that the CSCNT cathode exhibited a notably larger double-layer capacitance (C_{dl} , $2.57 \times 10^{-6}\text{ F}$) than the planar Pt electrode ($4.22 \times 10^{-8}\text{ F}$), suggesting a higher specific surface area in the former cathode. This is in accordance with the recent results of other nanostructured cathodes with a high porosity.^{58,59}

In order to get more information on the kinetics of the charge transfer reaction, EIS measurements have been performed at different temperatures ranging from $-10\text{ }^\circ\text{C}$ to $30\text{ }^\circ\text{C}$ with a temperature interval of $10\text{ }^\circ\text{C}$. Fig. 5(a) depicts the R_{ct} values as a function of the inverse of the absolute temperature. Remarkably, the CSCNT cathode yields a greatly decreased R_{ct} value compared to that of the Pt cathode, and the difference becomes more significant at low temperature. Furthermore, the exchange current density (J_0) can be calculated from the charge transfer resistance by:

$$J_0 = RT/nFR_{ct} \quad (1)$$

where R is the gas constant, T is the absolute temperature, n is the number of electrons being transferred during the disulfide-to-thiolate reduction process and F is the Faraday constant. J_0 is an important parameter describing the kinetics of the charge transfer reaction at the cathode–electrolyte interface. Assuming typical photocurrent densities for the TiO_2 photoanode working

Table 1 Fitted EIS parameters from the dummy cell and photovoltaic performance of DSCs with different cathodes in conjunction with a T⁻/T₂ electrolyte under 1 sun illumination (AM 1.5G, 100 mW cm⁻²)^a

Cathode	R_s [Ω cm ²]	R_{ct} [Ω cm ²]	C_{dl} [F]	V_{oc} [mV]	J_{sc} [mA cm ⁻²]	FF	PCE [%]
Pt	4.89 ± 0.18	12.55 ± 0.24	(4.22 ± 0.47) × 10 ⁻⁸	607 ± 3	13.85 ± 0.12	0.54 ± 0.02	4.54 ± 0.05
CSCNT	5.48 ± 0.23	1.26 ± 0.16	(2.57 ± 0.30) × 10 ⁻⁶	610 ± 3	14.25 ± 0.26	0.67 ± 0.01	5.81 ± 0.12

^a R_s = series resistance; R_{ct} = charge-transfer resistance; C_{dl} = double-layer capacitance; V_{oc} = open-circuit voltage; J_{sc} = short-circuit photocurrent density; FF = fill factor; PCE = power conversion efficiency. Values presented here are the average of at least three samples.

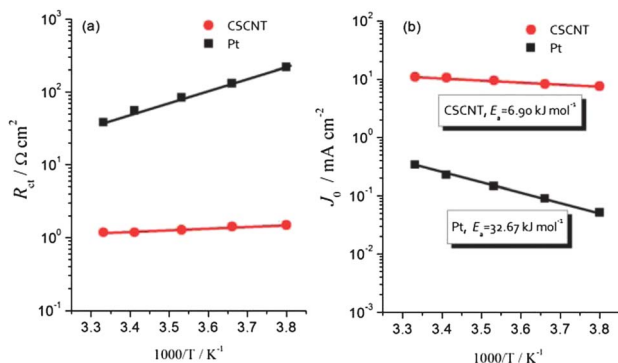


Fig. 5 Arrhenius plot of the charge transfer resistance (R_{ct} , a) and the exchange current density (J_0 , b). Insets of (b) show the derived apparent activation energies from the slopes of the Arrhenius plots.

under full sun illumination to be *ca.* 20 mA cm⁻², eqn (1) provides an estimated R_{ct} of 1.3 Ω cm² for the same J_0 value of the cathode. Such values are accessible for the I₃⁻/I⁻ redox couple electrolyte on a Pt cathode,^{55,60} but few catalysts exhibit comparable catalytic activities in recently investigated iodine-free electrolytes.^{20,61–63} As previously demonstrated, the R_{ct} of the CSCNT cathode is only 1.26 Ω cm², thus highlighting the unprecedented electrocatalytic activity of the CSCNT sheet towards disulfide-to-thiolate reduction. Normally, J_0 follows the Arrhenius equation:

$$J_0 = J_{inf} e^{-E_a/RT} \quad (2)$$

where J_{inf} is the exchange current density at infinite temperature and E_a is the apparent activation energy for the disulfide-to-thiolate reduction. The corresponding Arrhenius plots of the J_0 for CSCNT and the reference Pt cathode are shown in Fig. 5(b). Following eqn (2), the temperature-dependent measurements enable the calculation of E_a for the electron transfer process at the cathode interface. As indicated in the inset, the Pt cathode yields an apparent activation energy of 32.67 kJ mol⁻¹, which is in agreement with recent values derived by J. Burschka (30.9 kJ mol⁻¹).²² Spectacularly, the CSCNT cathode confers a greatly decreased apparent activation energy of only 6.90 kJ mol⁻¹, a value almost 4-fold lower than that of the Pt cathode. Such a value is of great advance, even compared with recently recognized highly efficient catalytic materials for disulfide/thiolate redox couples, such as CoS (33.8 kJ mol⁻¹) and porous PEDOT (37.8 kJ mol⁻¹).²² To the best of our knowledge, this is the first time that such a remarkably attenuated apparent activation energy than that of the conventional Pt cathode was obtained among various platinum-free alternatives.

The electrochemical stability of the CSCNT cathode in the electrolyte surroundings was further tested by consecutive measurements of the electrochemical impedance spectra of the CSCNT cathode at room temperature. The conventional Pt cathode was also tested as a control. As evidently depicted in Fig. 6, the CSCNT cathode survived this test without apparent changes in terms of serial resistance (R_s) and charge transfer resistance (R_{ct}) at the electrolyte–cathode interface, but the electrocatalytic activity of the Pt cathode decreased in each subsequent measurement. The R_{ct} for the Pt cathode, which was originally 12.55 Ω cm² in the first measurement, gradually increased up to 21.66 Ω cm² in the 10th cycle. On the other hand, the CSCNT cathode exhibited a stable R_{ct} of 1.26 Ω cm², independent of the measurement times. A possible reason for the deactivation of the Pt cathode in the sulfur-functionalized electrolyte with aging time is the specific adsorption of sulfur atoms on the cathode surface, and thus the reduced rate of catalytic reduction of the oxidized species at the platinum cathode.^{17,20,21} This experiment highlights the superior electrochemical stability of the CSCNT cathode in the disulfide/thiolate electrolyte. Recently, the electrochemical stability of a graphene nanoplatelet cathode was also tested by repeated measurements of electrochemical impedance after some time of aging at room temperature and the open circuit in a cobalt–bipyridine-mediated electrolyte.⁶³ However, to the best of our knowledge, this is the first report addressing the electrochemical stability of cathodes in disulfide/thiolate electrolytes, thus drawing special attention to the further exploration of alternative catalysts for these promising iodine-free redox couples.

The electrocatalytic activity of the CSCNT cathode toward the commonly-applied iodide electrolyte with a composition of 1.0 M 1,2-dimethyl-3-propylimidazolium iodide, 0.03 M I₂,

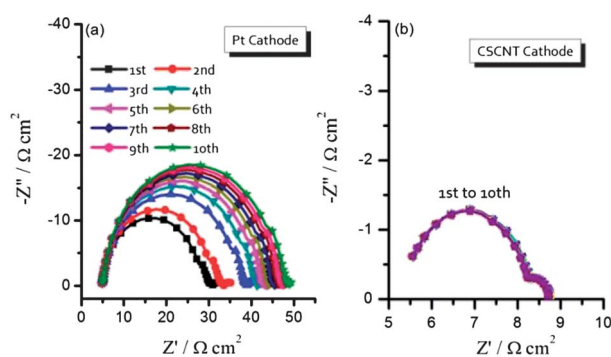


Fig. 6 Electrochemical stability of symmetrical dummy cells with Pt (a) and CSCNT cathode (b) in acetonitrile–ethylene carbonate solution of T₂T⁻. The EIS measurements were consecutively carried out at 0 V from 100 kHz to 1 Hz and repeated 10 times for each dummy cell.

0.5 M 4-*tert*-butylpyridine and 0.1 M guanidinium thiocyanate in dry acetonitrile was also investigated by using a symmetrical dummy cell. As depicted by the representative Nyquist spectra in Fig. 7, the conventional sputtered Pt electrode demonstrated a R_{ct} of $0.71 \Omega \text{ cm}^2$. Meanwhile, the CSCNT cathode exhibited a comparable electrocatalytic activity in conjunction with this iodide redox couple-containing electrolyte, yielding an R_{ct} of the magnitude of $1.00 \Omega \text{ cm}^2$. This is in agreement with our previous results on the CNT cathode toward iodide electrolyte,³⁷ revealing the wide applicability of the as-prepared CSCNT cathode. Considering the superior electrochemical activity of the CSCNT cathode with respect to the ubiquitous Pt cathode in the sulfide-mediated electrolyte, our investigation draws attention to the importance of suitable catalyst redox coupling for progress in developing low-cost and high-efficiency iodine-free DSCs.

To further confirm the superior electrocatalytic activity of the CSCNT cathode, DSC devices were assembled with N719-sensitized TiO_2 electrodes with a configuration of $8 \mu\text{m}$ transparent layer (20 nm particle diameter) and a $5 \mu\text{m}$ thick scattering layer (250 nm particle diameter) and an active area of 0.16 cm^2 . Fig. 8 demonstrates the characteristic J - V performance for devices with CSCNT and reference Pt cathodes measured under AM 1.5G illumination and the detailed photovoltaic parameters are tabulated in Table 1. Device A with a Pt cathode in conjunction with a T^-/T_2 electrolyte exhibits an open-circuit voltage (V_{oc}) of 607 mV, a short-circuit photocurrent density (J_{sc}) of 13.85 mA cm^{-2} , a fill factor (FF) of 0.54, yielding an overall power conversion efficiency (PCE) of 4.54%. Impressively, device B with CSCNTs displays a considerable increase in FF up to 0.67, accompanied with a J_{sc} of 14.25 mA cm^{-2} and a V_{oc} of 610 mV, and produces a PCE of 5.81%. Apparently, the enhancement of the PCE directly originates from the FF increase. It is widely recognized that the FF of a DSC device is governed by the total series resistance of the cell, including the sheet resistances of the substrate and cathode, the electron transport resistance through the photoanode, ion diffusion resistance in the electrolyte, and the charge-transfer resistance (R_{ct}) at the cathode.⁶⁴ Therefore, the FF enhancement in the current work is mainly a result of the superior electrocatalytic

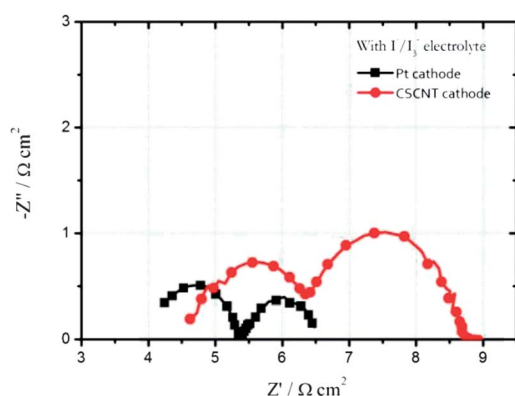


Fig. 7 Nyquist spectra of symmetrical dummy cells with CSCNT cathode and sputtered Pt electrode in conjunction with the iodide electrolyte of 1.0 M 1,2-dimethyl-3-propylimidazolium iodide, 0.03 M I_2 , 0.5 M 4-*tert*-butylpyridine and 0.1 M guanidinium thiocyanate in dry acetonitrile solution.

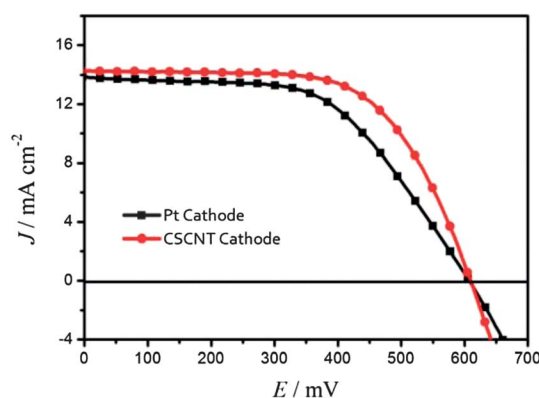


Fig. 8 Representative photocurrent–voltage characteristics of DSCs using CSCNT or Pt cathodes under 1 sun illumination (AM 1.5G, 100 mW cm^{-2}). The electrolyte was composed of 0.4 M T^- 0.4 M T_2 , 0.5 M 4-*tert*-butylpyridine, and 0.05 M LiClO_4 in acetonitrile : ethylene carbonate = 6 : 4 (volume ratio).

activity of the CSCNT cathode and the consequent significantly reduced charge-transfer resistance across the cathode–electrolyte interface. A significant improvement in charge transfer at the cathode–electrolyte interface not only reduces the internal resistances, but also attenuates the recombination rates and concentration gradients in the electrolyte, which proved to affect J_{sc} strongly.⁶⁵

4. Conclusions

In summary, we have developed CSCNT sheets as an efficient low-cost catalyst material in iodine-free DSCs, featuring a notably improved electrocatalytic activity toward the thiolate/disulfide redox shuttle. From the electrochemical characterization, the charge transfer resistance and apparent activation energy for disulfide reduction were only 10% and 25% of that with the Pt cathode. The excellent electrochemical stability of the CSCNT cathode in the disulfide/thiolate electrolyte has also been highlighted. Such a superior electrocatalytic activity was probably attributed to the synergistic effect of the high specific surface area, relatively open structure for electrolyte accessibility and defect-rich CSCNT cathode. Impressively, the device in conjunction with the CSCNT cathode demonstrates a higher FF and PCE with respect to that with a sputtered Pt cathode. Therefore, the highly catalytic CSCNT counter electrodes are identified to be a versatile alternative for the expensive and scarce platinum cathode in these iodine-free redox couple based DSCs.

Acknowledgements

Financial support from the National High Technology Research and Development Program of China (863 Program, 2011AA050522), and the International Cooperation S and T Cooperation Program of China (2010DFA64360, 2010DFA61410) is greatly appreciated.

Notes and references

- 1 N. S. Lewis and D. G. Nocera, *Proc. Natl. Acad. Sci. U. S. A.*, 2006, **103**, 15729–15735.
- 2 B. Oregan and M. Grätzel, *Nature*, 1991, **353**, 737–740.

- 3 U. Bach, D. Lupo, P. Comte, J. E. Moser, F. Weissortel, J. Salbeck, H. Spreitzer and M. Grätzel, *Nature*, 1998, **395**, 583–585.
- 4 M. Grätzel, *Nature*, 2001, **414**, 338–344.
- 5 Y. Chiba, A. Islam, Y. Watanabe, R. Komiya, N. Koide and L. Y. Han, *Jpn. J. Appl. Phys.*, 2006, **45**, L638–L640.
- 6 G. Boschloo and A. Hagfeldt, *Acc. Chem. Res.*, 2009, **42**, 1819–1826.
- 7 W. Kubo, S. Kambe, S. Nakade, T. Kitamura, K. Hanabusa, Y. Wada and S. Yanagida, *J. Phys. Chem. B*, 2003, **107**, 4374–4381.
- 8 S. Yanagida, Y. H. Yu and K. Manseki, *Acc. Chem. Res.*, 2009, **42**, 1827–1838.
- 9 A. M. Spokoyny, T. C. Li, O. K. Farha, C. W. Machan, C. X. She, C. L. Stern, T. J. Marks, J. T. Hupp and C. A. Mirkin, *Angew. Chem., Int. Ed.*, 2010, **49**, 5339–5343.
- 10 H. N. Tian, X. A. Jiang, Z. Yu, L. Kloo, A. Hagfeldt and L. C. Sun, *Angew. Chem., Int. Ed.*, 2010, **49**, 7328–7331.
- 11 Y. Bai, Q. J. Yu, N. Cai, Y. H. Wang, M. Zhang and P. Wang, *Chem. Commun.*, 2011, **47**, 4376–4378.
- 12 P. J. Cameron, L. M. Peter, S. M. Zakeeruddin and M. Grätzel, *Coord. Chem. Rev.*, 2004, **248**, 1447–1453.
- 13 T. W. Hamann and J. W. Ondersma, *Energy Environ. Sci.*, 2011, **4**, 370–381.
- 14 S. M. Feldt, E. A. Gibson, E. Gabrielsson, L. Sun, G. Boschloo and A. Hagfeldt, *J. Am. Chem. Soc.*, 2010, **132**, 16714–16724.
- 15 T. C. Li, A. M. Spokoyny, C. X. She, O. K. Farha, C. A. Mirkin, T. J. Marks and J. T. Hupp, *J. Am. Chem. Soc.*, 2010, **132**, 4580–4582.
- 16 T. Daeneke, T. H. Kwon, A. B. Holmes, N. W. Duffy, U. Bach and L. Spiccia, *Nat. Chem.*, 2011, **3**, 211–215.
- 17 M. K. Wang, N. Chamberland, L. Breau, J. E. Moser, R. Humphry-Baker, B. Marsan, S. M. Zakeeruddin and M. Grätzel, *Nat. Chem.*, 2010, **2**, 385–389.
- 18 H. N. Tian, E. Gabrielsson, Z. Yu, A. Hagfeldt, L. Kloo and L. C. Sun, *Chem. Commun.*, 2011, **47**, 10124–10126.
- 19 H. N. Tian, Z. Yu, A. Hagfeldt, L. Kloo and L. Sun, *J. Am. Chem. Soc.*, 2011, **133**, 9413–9422.
- 20 L. Wang, M. X. Wu, Y. R. Gao and T. L. Ma, *Appl. Phys. Lett.*, 2011, **98**, 221102.
- 21 H. W. Wu, Z. B. Lv, Z. Z. Chu, D. Wang, S. C. Hou and D. C. Zou, *J. Mater. Chem.*, 2011, **21**, 14815–14820.
- 22 J. Burschka, V. Brault, S. Ahmad, L. Breau, M. K. Nazeeruddin, B. Marsan, S. M. Zakeeruddin and M. Grätzel, *Energy Environ. Sci.*, 2012, **5**, 6089–6097.
- 23 S. Ahmad, J. H. Yum, H. J. Butt, M. K. Nazeeruddin and M. Grätzel, *ChemPhysChem*, 2010, **11**, 2814–2819.
- 24 X. Xin, M. He, W. Han, J. Jung and Z. Lin, *Angew. Chem., Int. Ed.*, 2011, **50**, 11739–11742.
- 25 S. I. Cha, B. K. Koo, S. H. Seo and D. Y. Lee, *J. Mater. Chem.*, 2010, **20**, 659–662.
- 26 M. Wu, X. Lin, Y. Wang, L. Wang, W. Guo, D. Qi, X. Peng, A. Hagfeldt, M. Grätzel and T. Ma, *J. Am. Chem. Soc.*, 2012, **134**, 3419–3428.
- 27 J. Velten, A. J. Mozer, D. Li, D. Officer, G. Wallace, R. Baughman and A. Zakhidov, *Nanotechnology*, 2012, **23**, 085201.
- 28 S. Roy, R. Bajpai, A. K. Jena, P. Kumar, N. Kulshrestha and D. S. Misra, *Energy Environ. Sci.*, 2012, **5**, 7001–7006.
- 29 S. J. Peng, P. N. Zhu, Y. Z. Wu, S. G. Mhaisalkar and S. Ramakrishna, *RSC Adv.*, 2012, **2**, 652–657.
- 30 D. Noureldine, T. Shoker, M. Musameh and T. H. Ghaddar, *J. Mater. Chem.*, 2012, **22**, 862–869.
- 31 K. S. Lee, Y. Lee, J. Y. Lee, J. H. Ahn and J. H. Park, *ChemSusChem*, 2012, **5**, 379–382.
- 32 B. Lee, D. B. Buchholz and R. P. H. Chang, *Energy Environ. Sci.*, 2012, **5**, 6941–6952.
- 33 G. Zhu, L. K. Pan, T. Lu, T. Xu and Z. Sun, *J. Mater. Chem.*, 2011, **21**, 14869–14875.
- 34 M. X. Wu, Y. D. Wang, X. Lin, N. S. Yu, L. Wang, L. L. Wang, A. Hagfeldt and T. L. Ma, *Phys. Chem. Chem. Phys.*, 2011, **13**, 19298–19301.
- 35 J. Han, H. Kim, D. Y. Kim, S. M. Jo and S. Y. Jang, *ACS Nano*, 2010, **4**, 3503–3509.
- 36 J. G. Nam, Y. J. Park, B. S. Kim and J. S. Lee, *Scr. Mater.*, 2010, **62**, 148–150.
- 37 P. Dong, C. L. Pint, M. Hainey, F. Mirri, Y. J. Zhan, J. Zhang, M. Pasquali, R. H. Hauge, R. Verduzco, M. A. Jiang, H. Lin and J. Lou, *ACS Appl. Mater. Interfaces*, 2011, **3**, 3157–3161.
- 38 C. T. Hsieh, B. H. Yang and J. Y. Lin, *Carbon*, 2011, **49**, 3092–3097.
- 39 M. Y. Yen, M. C. Hsiao, S. H. Liao, P. I. Liu, H. M. Tsai, C. C. M. Ma, N. W. Pu and M. D. Ger, *Carbon*, 2011, **49**, 3597–3606.
- 40 Z. Yang, T. Chen, R. He, G. Guan, H. Li, L. Qiu and H. Peng, *Adv. Mater.*, 2011, **23**, 5436–5439.
- 41 S. Q. Huang, L. Li, Z. B. Yang, L. L. Zhang, H. Saiyin, T. Chen and H. S. Peng, *Adv. Mater.*, 2011, **23**, 4707–4710.
- 42 X. Mei, S. J. Cho, B. Fan and J. Ouyang, *Nanotechnology*, 2010, **21**, 395202.
- 43 K. S. Lee, W. J. Lee, N. G. Park, S. O. Kim and J. H. Park, *Chem. Commun.*, 2011, **47**, 4264–4266.
- 44 S. S. Li, Y. H. Luo, W. Lv, W. J. Yu, S. D. Wu, P. X. Hou, Q. H. Yang, Q. B. Meng, C. Liu and H. M. Cheng, *Adv. Energy Mater.*, 2011, **1**, 486–490.
- 45 F. Hao, P. Dong, J. Zhang, Y. Zhang, P. E. Loya, R. H. Hauge, J. Li, J. Lou and H. Lin, *Sci. Rep.*, 2012, **2**, 368.
- 46 K. L. Jiang, Q. Q. Li and S. S. Fan, *Nature*, 2002, **419**, 801.
- 47 H. X. Zhang, C. Feng, Y. C. Zhai, K. L. Jiang, Q. Q. Li and S. S. Fan, *Adv. Mater.*, 2009, **21**, 2299–2304.
- 48 For a brief review, please see: K. L. Jiang, J. P. Wang, Q. Q. Li, L. A. Liu, C. H. Liu and S. S. Fan, *Adv. Mater.*, 2011, **23**, 1154–1161.
- 49 X. B. Zhang, K. L. Jiang, C. Teng, P. Liu, L. Zhang, J. Kong, T. H. Zhang, Q. Q. Li and S. S. Fan, *Adv. Mater.*, 2006, **18**, 1505–1510.
- 50 F. Hao, H. Lin, C. Zhou, Y. Z. Liu and J. B. Li, *Phys. Chem. Chem. Phys.*, 2011, **13**, 15918–15924.
- 51 K. Liu, Y. H. Sun, P. Liu, X. Y. Lin, S. S. Fan and K. L. Jiang, *Adv. Funct. Mater.*, 2011, **21**, 2721–2728.
- 52 T. Jawhari, A. Roid and J. Casado, *Carbon*, 1995, **33**, 1561–1565.
- 53 W. J. Lee, E. Ramasamy, D. Y. Lee and J. S. Song, *ACS Appl. Mater. Interfaces*, 2009, **1**, 1145–1149.
- 54 C. E. Banks, T. J. Davies, G. G. Wildgoose and R. G. Compton, *Chem. Commun.*, 2005, 829–841.
- 55 A. Hauch and A. Georg, *Electrochim. Acta*, 2001, **46**, 3457–3466.
- 56 Q. Wang, S. Ito, M. Grätzel, F. Fabregat-Santiago, I. Mora-Sero, J. Bisquert, T. Bessho and H. Imai, *J. Phys. Chem. B*, 2006, **110**, 25210–25221.
- 57 J. E. Trancik, S. C. Barton and J. Hone, *Nano Lett.*, 2008, **8**, 982–987.
- 58 W. J. Lee, E. Ramasamy, D. Y. Lee and J. S. Song, *ACS Appl. Mater. Interfaces*, 2009, **1**, 1145–1149.
- 59 P. Joshi, L. F. Zhang, Q. L. Chen, D. Galipeau, H. Fong and Q. Q. Qiao, *ACS Appl. Mater. Interfaces*, 2010, **2**, 3572–3577.
- 60 L. Kavan, J. H. Yum, M. K. Nazeeruddin and M. Grätzel, *ACS Nano*, 2011, **5**, 9171–9178.
- 61 L. Wang, E. W. G. Diau, M. X. Wu, H. P. Lu and T. L. Ma, *Chem. Commun.*, 2012, **48**, 2600–2602.
- 62 H. N. Tsao, J. Burschka, C. Y. Yi, F. Kessler, M. K. Nazeeruddin and M. Grätzel, *Energy Environ. Sci.*, 2011, **4**, 4921–4924.
- 63 L. Kavan, J. H. Yum and M. Grätzel, *Nano Lett.*, 2011, **11**, 5501–5506.
- 64 T. W. Hamann, R. A. Jensen, A. B. F. Martinson, H. Van Ryswyk and J. T. Hupp, *Energy Environ. Sci.*, 2008, **1**, 66–78.
- 65 Z. Tachan, M. Shalom, I. Hod, S. Ruhle, S. Tirosch and A. Zaban, *J. Phys. Chem. C*, 2011, **115**, 6162–6166.